Journal of Materials Chemistry A

Effects of End-On Oriented Polymer Chains at the Donor/Acceptor Interface in Organic Solar Cells

Journal:	*Journal of Materials Chemistry A*
Manuscript ID	TA-ART-09-2018-009307.R1
Article Type:	Paper
Date Submitted by the Author:	25-Oct-2018
Complete List of Authors:	Wang, Fanji; RIKEN Center for Emergent Matter Science (CEMS), Supramolecular Chemistry Division Nakano, Kyohei; RIKEN, Center for Emergent Matter Science Yoshida, Hiroyuki; Chiba University, Graduate School of Advanced Integration Science Hashimoto, Kazuhito; The University of Tokyo, Research Centre for Advanced Science and Technology Segawa, Hiroshi; The University of Tokyo, Research Center for Advanced Science and Technology Hsu, Chain Shu; National Chiao Tung University, Tajima, Keisuke; RIKEN Center for Emergent Matter Science (CEMS), Supramolecular Chemistry Division

Journal Name

ARTICLE

Effects of End-On Oriented Polymer Chains at the Donor/Acceptor Interface in Organic Solar Cells

Received 00th January 20xx,
Accepted 00th January 20xx

DOI: 10.1039/x0xx00000x

www.rsc.org/

Fanji Wang,[ab] Kyohei Nakano,[a] Hiroyuki Yoshida,[cd] Kazuhito Hashimoto,[b] Hiroshi Segawa,[ef] Chain-Shu Hsu[g] and Keisuke Tajima*[a]

Molecular alignment at the interface between the electron donor and acceptor (D/A) materials in thin films may have a large effect on the charge generation process in organic solar cells (OSCs). In this study, the effects of the polymer chain orientations at the D/A interface were investigated in OSCs with planar heterojunction (PHJ) structures. Poly(3-alkylthiophene) films with edge-on (main chain parallel to the interface) and end-on (main chain vertical to the interface) orientations at the surface were used to construct PHJs with a fullerene derivative. Ultraviolet photoelectron spectroscopy and low-energy inverse photoelectron spectroscopy revealed that the difference in polarization energy through the charge-permanent quadrupole interaction causes a rigid energy shift of 0.5 eV between the two orientations. The PHJ device with the end-on oriented polymer chains at the D/A interface showed a smaller photovoltage loss expected from the energy structure and a more efficient charge separation than the device with the edge-on oriented polymer chains. These improvements were attributed to charge delocalization along the end-on oriented polymer chains normal to the D/A interface, through which the effective binding energy of the charge pairs in the interfacial charge-transfer state was reduced. These results provide important information about molecular arrangements at the D/A interface that may enable further improvements in OSC performance.

Introduction

The performance of solution-processed organic solar cells (OSCs) has been improved substantially based on mixed bulk heterojunction (BHJ) structures and the power conversion efficiency (PCE) of OSCs has already exceeded 12%.[1-5] Nevertheless, the mechanism for efficient charge generation in OSCs despite the strong Coulombic interaction originating from the low dielectric constants of the organic materials is not fully understood.[6-7] It has been proposed that entropic gain,[8-10] thermally non-equilibrated "hot" processes,[11-14] charge delocalization,[15-22] and interfacial cascade structures[23-28] play key roles in the mechanism. Among them, the effect of the delocalized nature of the charge pairs at the donor/acceptor (D/A) interfaces has previously been investigated by using transient optical measurements.[15-19] Both the intra- and intermolecular charge delocalization can weaken the effective Coulombic binding of the charge pairs and facilitate the dissociation of the interfacial charge-transfer state (CTS). This suggests that the relative orientation between the donor and the acceptor molecules may be important for efficient charge separation because the shapes of the molecules and the molecular orbitals (MOs) are generally anisotropic.

Mixed BHJ structures are not suitable for experimental investigation of the molecular orientation because the molecular positions and the orientations are poorly controlled in the randomly mixed films. However, planar heterojunction (PHJ) structures are suitable for this purpose because the donor and acceptor are in separate layers, and the relative orientation is well defined by the molecular orientations to the interfacial plane.[29] Several studies on the effects of the molecular orientation in PHJs have previously been reported.[30-38] Among them, the effects of the chain orientation of π-conjugated polymers at the D/A interface are of particular interest because of their highly anisotropic structures and excellent performance in mixed BHJs.[35-38] However, studies are so far limited to the comparison of edge-on (main chain parallel and π-plane vertical to the D/A interface) and face-on (main chain and π-plane parallel to the D/A interface) orientations of the donor polymers. Because the charges are mainly delocalized along the polymer main chain,

[a] RIKEN Center for Emergent Matter Science (CEMS), 2-1 Hirosawa, Wako, Saitama 351-0198, Japan.* E-mail: keisuke.tajima@riken.jp
[b] Department of Applied Chemistry Graduate School of Engineering, The University of Tokyo, 7-3-1 Hongo, Bunkyo-ku, Tokyo 113-8656, Japan
[c] Graduate School of Engineering, Chiba University, 1-33 Yayoi-cho, Inage-ku, Chiba-shi, Chiba 263-8522, Japan
[d] Molecular Chirality Research Center, Chiba University, 1-33 Yayoi-cho, Inage-ku, Chiba-shi, Chiba 263-8522, Japan
[e] Research Center for Advanced Science and Technology, The University of Tokyo, 4-6-1 Komaba, Meguro-ku, Tokyo 153-8904, Japan
[f] Graduate School of Arts and Sciences, The University of Tokyo, 3-8-1 Komaba, Meguro-ku, Tokyo 153-8902, Japan
[g] Department of Applied Chemistry, National Chiao Tung University, 1001 University Road, Hsinchu 30010, Taiwan
†Electronic Supplementary Information (ESI) available. See DOI: 10.1039/x0xx00000x

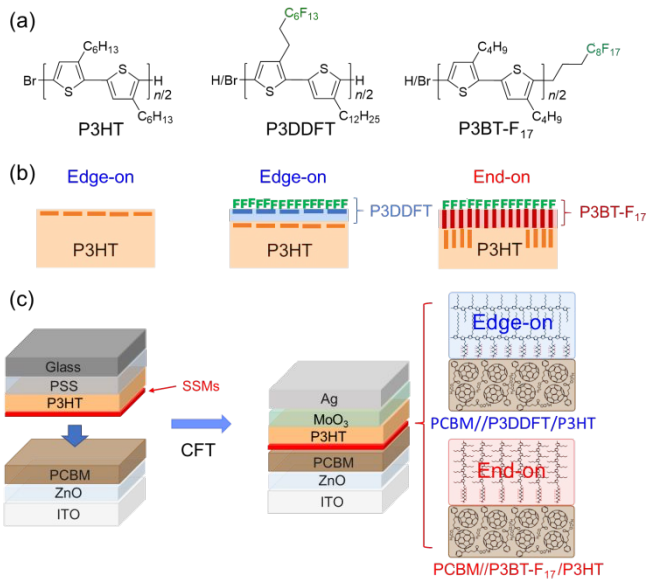

Figure 1. (a) Chemical structures of the poly(3-alkylthiophene)s used in this study. (b) Schematics of the P3HT, P3DDFT/P3HT, and P3BT-F_{17}/P3HT donor films. (c) Schematic of the fabrication process for the PHJ devices by CFT. The interfacial orientations of polymers are edge-on for PCBM//P3DDFT/P3HT and end-on for PCBM//P3BT-F_{17}/P3HT, where // denotes the interface made by CFT.

both the orientations could produce similar Coulombic binding of the charge pair, with the positive charge delocalized laterally to the interfacial plane of the CTS. We hypothesize that the end-on orientation (main chain vertical to the D/A interface) could have the delocalized positive charge perpendicular to the interfacial plane. This orientation should greatly reduce the binding energy in the CTS through the weakened Coulombic interaction with the longer effective charge distance, thus improving the OSC performance. The end-on orientation of the polymers at D/A interface and its effects on the charge generation processes have yet to be reported.

In this study, three polymer films with either edge-on or end-on orientations at the surface were prepared and evaluated (Figures 1a and b). Pristine P3HT film has the edge-on orientation at the surface owing to the low surface energy of the linear alkyl chains.[39] We previously developed polymer-based surface-segregated monolayers (SSMs) to control the polymer alignments at the film surface.[40-45] During spin-coating, both P3DDFT and P3BT-F_{17} with semifluoroalkyl groups at the side chains and at one end of the main chain, respectively, segregate on top of the thin films to form monolayers with controlled molecular orientations. Due to the different positions of the semifluoroalkyl groups with low surface energy, P3DDFT adopts the edge-on orientation at the surface of the P3HT film after spin-coating from the mixed solution (P3DDFT/P3HT, Figure 1b),[40-42] whereas P3BT-F_{17} adopts the end-on orientation (P3BT-F_{17}/P3HT, Figure 1b).[41-43] The effects of the chain orientation and molecular dipole moments on the ionization energy (IE) and electron affinity (EA) are quantitatively determined by ultraviolet photoelectron spectroscopy (UPS) and low-energy inverse photoelectron spectroscopy (LEIPS), respectively. In addition, the contact film transfer (CFT) method allows us to transfer the polymer films onto [6,6]-phenyl-C_{61}-butyric acid methyl ester (PCBM) film without using heat, pressure, or organic solvents, leading to the formation of a well-defined D/A interface suitable for PHJs.[39, 46-47] We compared the electronic structures, light absorption, exciton diffusion, charge separation and recombination processes of the PHJ devices with the structures of PCBM//P3DDFT/P3HT and PCBM//P3BT-F_{17}/P3HT, which had edge-on and end-on orientations, respectively, at the D/A interface (Figure 1c).

Results and discussion

The surface segregation behavior of P3DDFT and P3BT-F_{17} in P3HT films was investigated by X-ray photoelectron spectroscopy (XPS), which reproduced previous results.[40-43] The details of the measurements are summarized in Supporting Information (Section S1). The concentrations of P3DDFT and P3BT-F_{17} in blend solutions with P3HT were optimized to be P3DDFT (0.6 mg mL^{-1})/P3HT (7.0 mg mL^{-1}) and P3BT-F_{17} (2.6 mg mL^{-1})/P3HT (5.0 mg mL^{-1}) to achieve the maximum surface coverages of the SSMs over 95% with high surface F/C atomic ratios, based on an idealized bilayer model with complete coverage.[40-43] A pristine P3HT film (7.6 mg mL^{-1}) was also prepared as the control sample without the SSMs. Similar film thicknesses of 66, 63, and 65 nm were determined by X-ray reflectivity (XRR) for the P3HT, P3DDFT/P3HT and P3BT-F_{17}/P3HT films, respectively (Figure S2). The surface roughnesses of the three films were also similar, with arithmetic mean roughnesses (R_a) of 1.39–1.83 nm measured by atomic force microscopy (AFM) (Figure S3). These conditions were used for the subsequent experiments.

The molecular orientations in the three films were evaluated by in-plane and out-of-plane X-ray diffraction (XRD), 2D grazing-incidence wide-angle X-ray scattering (GIWAXS), and UV-vis absorption spectroscopy in transmittance mode (Figure 2). The P3HT and P3DDFT/P3HT films exhibited similar diffraction patterns in both XRD and GIWAXS, indicating that P3DDFT on the surface had little effect on the chain order of P3HT in the bulk (Figure 2a, b, d and e). The diffraction peaks at low q_{xy} and q_z of around 0.38 $Å^{-1}$ were assigned to the lamellar structure of P3HT, and their larger intensity in the out-of-plane direction than in the in-plane direction suggested that the edge-on orientation was dominant in the bulk of the P3HT and P3DDFT/P3HT films. The polymer chains on the surface of P3HT and P3DDFT/P3HT films also adopt the edge-on orientation due to the low surface energy of the linear alkyl and semifluoroalkyl chains.[39, 41, 43] The P3HT and P3DDFT/P3HT films showed similar UV-vis absorption spectra, including the absorption coefficients (Figure 2c), which reflected the similar chain orientations.

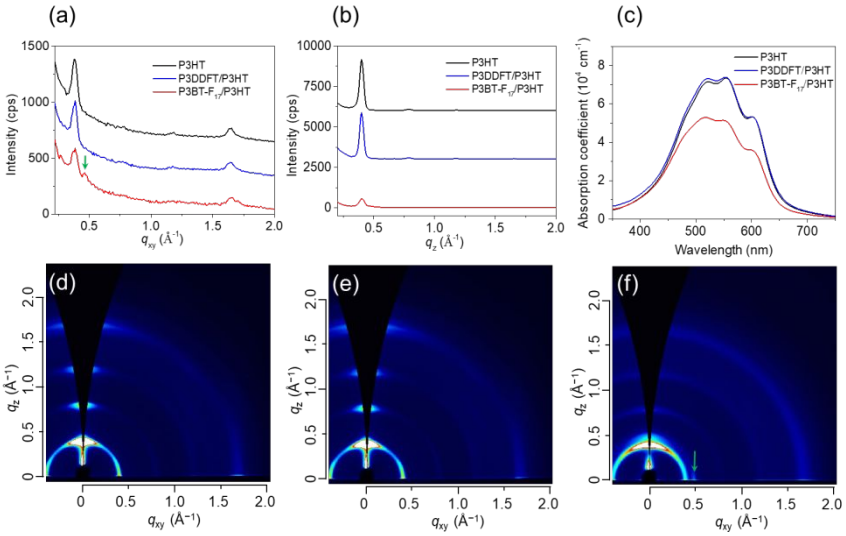

Figure 2. (a) In-plane and (b) out-of-plane XRD patterns, and (c) absorption coefficient spectra of P3HT (black), P3DDFT/P3HT (blue), and P3BT-F_{17}/P3HT (red) films. 2D GIWAXS patterns of (d) P3HT, (e) P3DDFT/P3HT, and (f) P3BT-F_{17}/P3HT films. The green arrows in (a) and (f) show the lamellar structure peak of P3BT-F_{17} in the in-plane direction, which indicates the formation of end-on oriented packing at the film surface.

In contrast, the P3BT-F_{17}/P3HT film showed a clear diffraction peak at 0.46 $Å^{-1}$ (13.6 Å) from the P3BT-F_{17} lamellar structure in the in-plane directions in the XRD and GIWAXS patterns in addition to the peak from the lamellar structure of P3HT (Figures 2a and f). These results are consistent with the formation of the ordered SSM with the end-on P3BT-F_{17} at the film surface as previously reported.[40-41] In addition, for the P3BT-F_{17}/P3HT film, the intensity of the P3HT lamellar peak in the out-of-plane direction was lower and the peak for the lamellar order of P3HT was broader in the GIWAXS patterns compared with P3HT and P3DDFT/P3HT films (Figures 2b and f). The UV-vis absorption spectrum of the P3BT-F_{17}/P3HT film had a similar shape but a much lower absorption coefficient compared with the other two films (Figure 2c). This was attributed to the large fraction of vertically oriented main chains in the film, which weakens the interaction between the electric field of normal incident light and the transition dipole moment of the molecules.[41] These results suggest that end-on oriented P3BT-F_{17} on the film surface affects the orientation order of P3HT in the bulk and induces a greater proportion of P3HT chains to be vertically oriented.[40] Note that the weaker light absorption of the end-on oriented P3BT-F_{17}/P3HT is detrimental for OSCs.

The introduction of the semifluoroalkyl chains and the difference in the chain orientations can change the electronic structure of the films through many factors, such as surface dipole moments, polarization energy, and intermolecular interactions.[48] The energy levels of the three films were determined by UPS and LEIPS[49-52] (Figure 3a). From the cut-off energy of the secondary electrons in UPS, the vacuum levels (E_{vac}) of the P3HT, P3DDFT/P3HT, and P3BT-F_{17}/P3HT films were determined to be 3.45, 4.50, and 4.51 eV, respectively, with respect to the Fermi level (E_F). The shifts (Δ) of E_{vac} from the P3HT film for P3DDFT/P3HT and P3BT-F_{17}/P3HT films were 1.05 and

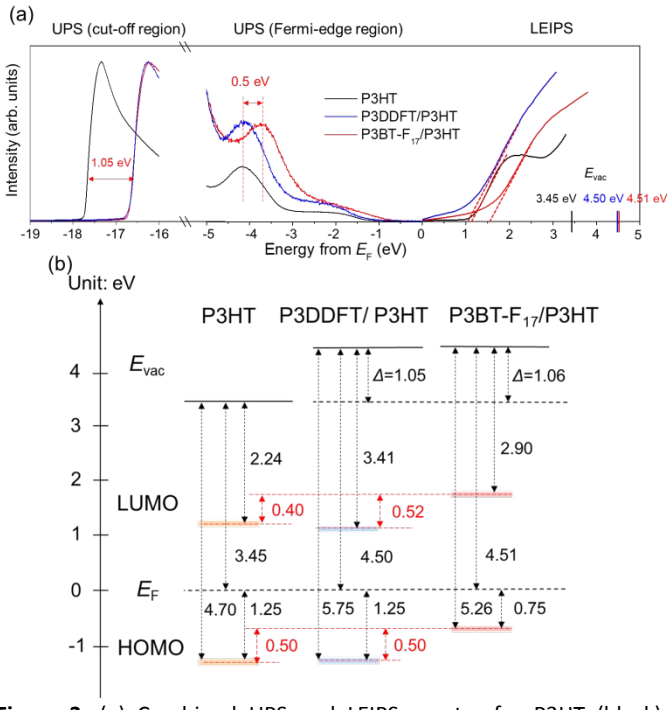

Figure 3. (a) Combined UPS and LEIPS spectra for P3HT (black), P3DDFT/P3HT (blue), and P3BT-F_{17}/P3HT (red) films with respect to E_F. (b) Energy level diagram of P3HT, P3DDFT/P3HT, and P3BT-F_{17}/P3HT films. Δ and the numbers in red represent the vacuum level shift and the orientation-dependent energy shift, respectively.

1.06 eV, respectively, which originated from the surface dipole layer formed by the aligned permanent dipole moments of the semifluoroalkyl chains in the SSMs.[27, 42-43, 47] The similar *Δ* values indicated similar dipole effects on the electronic structures of P3DDFT and P3BT-F_{17} at the surface of the P3HT layers.

The UPS spectrum in the Fermi-edge region showed two peaks around −2 and −4 eV with respect to the E_F (Figure 3a). According to density functional theory (DFT) calculations on a model oligomer of P3HT, the broad feature around −2 eV arose from intrachain band dispersion consisting of several delocalized polythiophene MOs with the onset derived from the highest occupied molecular orbital (HOMO). The second sharp peak originated from the degenerated polythiophene MOs with smaller delocalization (Figure S4). The positions of the two peaks for the P3HT and P3DDFT/P3HT films were similar. In contrast, both peaks for the P3BT-F_{17}/P3HT film showed a shift in the higher-energy direction of approximately 0.5 eV compared with the P3HT and P3DDFT/P3HT films. IEs were determined from the onset energy of the HOMO-derived band with respect to E_{vac} as 4.70, 5.75, and 5.26 eV for the P3HT, P3DDFT/P3HT, and P3BT-F_{17}/P3HT films, respectively.

The LEIPS spectra of P3HT and P3DDFT/P3HT showed rising signals with onsets at around 1 eV with respect to the E_F, which were assigned to the lowest unoccupied molecular orbital (LUMO)-derived bands (Figure 3a). The onset for the P3BT-F_{17}/P3HT film showed a shift in the higher-energy direction of approximately 0.5 eV compared with P3HT and P3DDFT/P3HT. The EA was determined from the onset energy of the LUMO-derived band with respect to E_{vac} of each film. To eliminate systematic error and determine the EA accurately,[49] the LEIPS spectra were measured with three different photon emission energies (Section S2, see details in the Supporting Information). The EAs of the P3HT, P3DDFT/P3HT, and P3BT-F_{17}/P3HT films were calculated to be 2.24, 3.41, and 2.90 eV, respectively.

The IEs, EAs, and E_{vac} of the three films with respect to the E_F are summarized in Figure 3b. The P3DDFT/P3HT film had a similar electronic structure to the pristine P3HT film, except for a *Δ* value of 1.05 eV due to the surface dipole moment of the semifluoroalkyl chains. In contrast, the P3BT-F_{17}/P3HT film showed a similar *Δ* value but an upward energetic shift in both IE and EA of approximately 0.5 eV compared with the other two films. Because UPS and LEIPS only detect the surface region of the films, these results indicate that the electronic structure of the poly(3-alkylthiophene) with the end-on orientation was different from that with the edge-on orientation. The dependence of electronic energy levels on the molecular orientation has previously been observed in films of semiconducting small molecules[48, 53-55] and theoretically explained by an electrostatic model.[49, 54-56] The rigid energetic shift caused by the orientation change of the molecules was attributed to the difference in the electrostatic polarization energy, which can be approximated by the charge-permanent quadrupole interactions in thin films.[48, 55-57] Therefore, assuming that the HOMO and LUMO energy levels of the polymer molecules and the intermolecular interactions in the films were the same for P3HT, P3DDFT, and P3BT-F_{17}, the change in Figure 3b can be simply separated into the following two independent factors: (1) The vacuum level shift (*Δ*) caused by the surface dipole with no change in energy levels with respect to E_F[43] and (2) the rigid shift of the energy levels with respect to E_F caused by the orientation effect with no change in the vacuum level.[48] This orientation effect has been predicted for vertically oriented semiconducting polymers in thin films, but this is the first experimental observation. Further discussion of the energy structures based on the SSM coverage dependence of the IE shifts, and the electrostatic energy calculations using the charge-permanent quadrupole interaction model are provided in Supporting Information (Section S3).

To obtain the actual energy diagrams for PHJs with the acceptor layer, we further considered the interfacial energy level alignments modified by the interfacial dipoles and the charge accumulations in the layers (i.e., band bending). We investigated the change in the cut-off energy of the secondary electrons in the

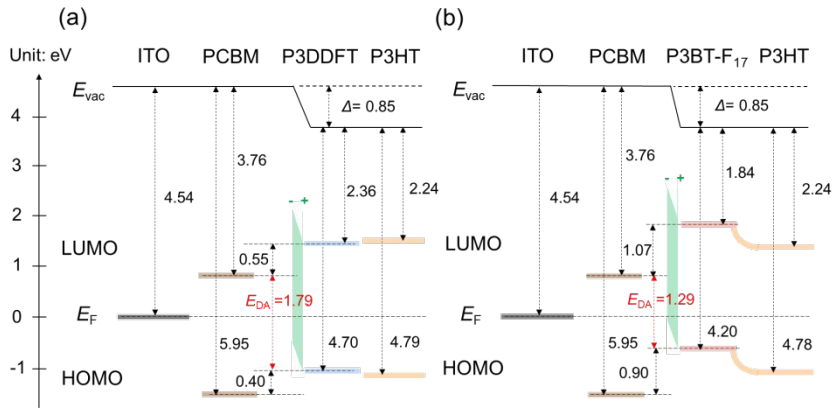

Figure 4. Energy diagrams of (a) PCBM//P3DDFT/P3HT and (b) PCBM//P3BT-F_{17}/P3HT. The E_{DA} in the two PHJs is shown in red.

UPS spectra of a pristine PCBM film and PCBM//polymer PHJ films on an indium tin oxide (ITO) substrate (Figure S11). The PCBM//P3DDFT/P3HT and PCBM//P3BT-F_{17}/P3HT PHJ films were prepared by transferring the corresponding polymer films onto the PCBM layer. Our previous study indicated that the D/A interface of PHJs prepared by CFT is well-defined with negligible intermixing, so the surface structures of the donor films are retained at the D/A interface after the film transfer.[27, 47, 58] Therefore, the edge-on and end-on oriented polymer chains were maintained at the D/A interfaces of PCBM//P3DDFT/P3HT and PCBM//P3BT-F_{17}/P3HT PHJs, respectively (Figure 1c).

The cut-off energy of secondary electrons in UPS showed that E_{vac} of both PCBM//P3DDFT/P3HT and PCBM//P3BT-F_{17}/P3HT films are shifted to the lower-energy side by 0.85 eV from that of the pristine PCBM film (Figure S11). As mentioned above, the large permanent dipole moments of the semifluoroalkyl chains in P3DDFT and P3BT-F_{17} lead to Δ of 1.05–1.06 eV at the film surfaces, which mainly contributes to the observed Δ (0.85 eV) at the organic interface in PHJs. The reduction of Δ by about 0.2 eV in the PHJ films can be ascribed to the depolarization owing to the existence of acceptor layer changing the effective dielectric constant approximately from 2 to 3.5 (see the model below).

To support our experimental results, an electrostatic numerical calculation based on the report by Oehzelt et al.[59] was performed for the film structures of PCBM//P3DDFT/P3HT and PCBM//P3BT-F_{17}/P3HT. The calculated energy values quantitatively reproduced the observed energy parameters, confirming the validity of this model calculation (Section S5, see details in the Supporting Information). Contributions to the shift of E_{vac} from the band bending by charge transfer were small for both structures, suggesting that the observed Δ was mainly caused by the interfacial dipole moment of the semifluoroalkyl chains.

Based on these results, energy diagrams for the PHJs could be constructed (Figure 4). IE (Figure S11) and EA[51] of the pristine PCBM film were 5.95 and 3.76 eV, respectively. The energy levels of the P3DDFT and P3BT-F_{17} layers in the PHJs were taken from the single films (Figure 3b) with an interfacial dipole moment correction of 0.85 eV. For PCBM//P3BT-F_{17}/P3HT, the orientation of the P3HT in the bulk of the films could change from end-on at the PCBM//P3BT-F_{17} interface to the edge-on at the surface, resulting in the change of the IE from 4.20 to 4.78 eV and the EA from 1.84 to 2.24 eV with respect to E_{vac}. These changes are shown as the bending of the HOMO and LUMO of P3HT in Figure 4b. From the energy diagrams, the differences between the IE of the donor and the EA of the acceptor (E_{DA}) were estimated as 1.79 and 1.29 eV for PCBM//P3DDFT/P3HT and PCBM//P3BT-F_{17}/P3HT, respectively (Table 1). E_{DA} can be regarded as the energy of the free charge pairs (i.e., charge-separated state) in the PHJs. We used the IE of P3BT-F_{17} to evaluate E_{DA} rather than that of P3HT because the P3BT-F_{17} interfacial layer was near the D/A interface with a thickness of ~8 nm, which should play a major role in the charge generation process.

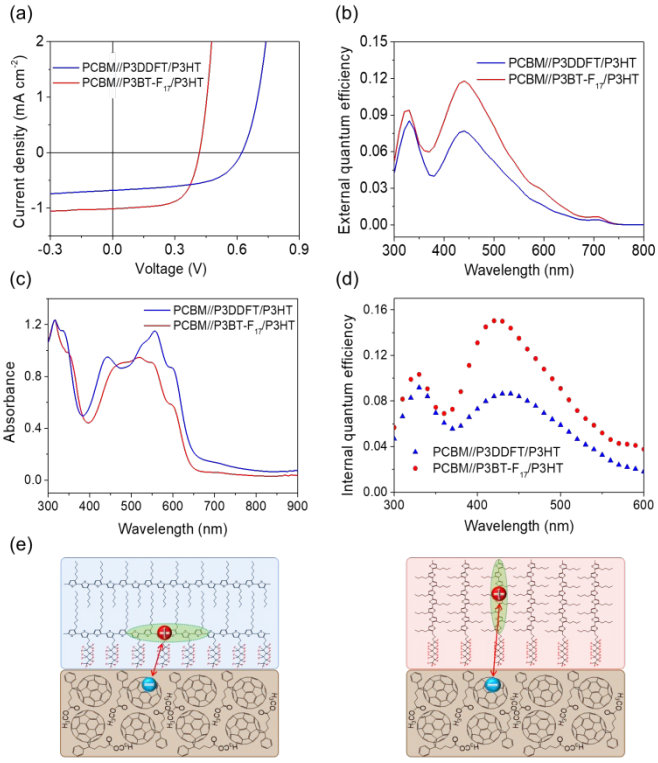

Figure 5. (a) *J-V* curves, (b) EQE spectra, (c) reflective UV-vis spectra, and (d) IQE spectra of two bilayer OSCs of PCBM//P3DDFT/P3HT (blue) and PCBM//P3BT-F_{17}/P3HT (red). In the IQE spectra, wavelengths above 600 nm are not shown owing to the inaccuracy caused by the low EQE signal and large background noise in the reflective spectra. (e) Schematic of the spatial delocalization of bound hole-electron pairs in the CTS of PHJ devices with edge-on and end-on polymers at the D/A interface. Green ellipses extended along the polymer main chains represent the intramolecular delocalization of the holes.

To complete the fabrication of the PHJ devices, MoO_3 and Ag were thermally evaporated onto the PHJ structures. The final device structure was glass/ITO/ZnO/PCBM//SSM/P3HT/MoO_3/Ag, where // denotes the interface created by the CFT method (Figure 1c). The *J-V* characteristics of the PHJ devices with the structures of PCBM//P3DDFT/P3HT and PCBM//P3BT-F_{17}/P3HT under AM1.5 (100 mW cm^{-2}) irradiation are shown in Figure 5a and the photovoltaic performances are summarized in Table 1.

Firstly, we correlated the interfacial energetics of PHJs with the observed difference in open circuit voltage (V_{OC}) of the OSCs. The energy loss from the charge separated state to the photovoltages (E_{DA}–eV_{OC}) was different in the two PHJ devices (1.17 eV for PCBM//P3DDFT/P3HT and 0.87 eV for PCBM//P3BT-F_{17}/P3HT). This difference indicates that the edge-on and the end-on molecular orientations at the D/A interface affect the loss process. It has been proposed that V_{OC} has a more direct correlation with interfacial CTS energy (E_{CT}) of

$$eV_{OC} = E_{CT} - nkT\ln(J_{00}/J_{ph}(V_{OC})) \quad (1)$$

where *e* is the elementary charge, *n* is the ideality factor, *k* is the Boltzmann constant, *T* is the temperature, J_{00} is the pre-exponential factor for the reverse saturation current density, and $J_{ph}(V_{OC})$ is the photogeneration rate of the charge density under open circuit conditions. E_{CT} can be obtained experimentally from the low-temperature limit of V_{OC} and the second term is the voltage loss determined by the balance between the charge generation and the bimolecular recombination rates in the film. We performed variable temperature measurements of V_{OC} under white LED light irradiation (Figure S13). The slopes of the V_{OC}-*T* curves were similar, suggesting the voltage loss due to the charge generation/recombination kinetics was similar in both devices. E_{CT} values extrapolated from the low-temperature limits of V_{OC} for PCBM//P3DDFT/P3HT and PCBM//P3BT-F_{17}/P3HT devices were 1.13 and 0.95 eV, respectively (Table 1).

E_{CT} can be expressed with E_{DA} as

$$E_{CT} = E_{DA} - E_b \quad (2)$$

where E_b is the Coulombic binding energy of the electron-hole pair in CTS. E_b values calculated from the experimental results were 0.66 and 0.34 eV for PCBM//P3DDFT/P3HT and PCBM//P3BT-F_{17}/P3HT, respectively (Table 1). Thus, PCBM//P3BT-F_{17}/P3HT with the end-on oriented polymer chains at the D/A interface had a considerably lower E_b than that of PCBM//P3DDFT/P3HT. In CTS at the D/A interface, the intrachain charge delocalization of the hole along the polymer backbone was predicted (Figure 5e). Therefore, the vertical delocalization of the hole in the PCBM//P3BT-F_{17}/P3HT device was expected to have a larger effective distance and weaker Coulombic interaction in CTS than that in the PCBM//P3DDFT/P3HT device with the edge-on orientation. This could lead to a smaller loss of photovoltage in PCBM//P3BT-F_{17}/P3HT device.

To support this difference in the CTS energy, we conducted time-dependent DFT calculations of the model interfaces for the edge-on and the end-on orientations (Section S6, see details in the Supporting Information). We assumed that the lowest excited states with the intermolecular charge transfer property were relevant to the charge separation. The calculations with different intermolecular distances and functionals gave us a consistent result. At the same distance, the end-on orientation gave a higher electronic energy for the CTS than the edge-on orientation, which supported the weaker Coulombic interaction in the CTS with the end-on orientation.

The weaker Coulombic interaction in the CTS with the end-on orientation could also facilitate the dissociation of the charge pairs. Therefore, we examined the charge generation process in the OSCs. The observed short-circuit current densities (J_{SC}) of the PCBM//P3DDFT/P3HT and PCBM//P3BT-F_{17}/P3HT devices were 0.67 and 1.03 mA cm^{-2}, respectively (Figure 5a and Table 1). Interestingly, despite the lower absorption coefficient of the P3BT-F_{17}/P3HT film (Figure 2c), J_{SC} of the PCBM//P3BT-F_{17}/P3HT device was much higher than that of the PCBM//P3DDFT/P3HT device. This result indicates that the end-on oriented polymer chains at the D/A interface could be advantageous for charge generation.

To confirm this, the charge generation efficiency was evaluated quantitatively. The external quantum efficiency (EQE) spectra of the two devices are shown in Figure 5b. The PCBM//P3BT-F_{17}/P3HT device exhibited a higher EQE over the entire spectrum compared with the PCBM//P3DDFT/P3HT device. The photocurrents calculated from the EQE results corresponded well to the J_{SC} measured under simulated solar light irradiation. UV-vis

Table 1. Summary of the photovoltaic performance for the two PHJ devices.

	V_{OC} (V)	J_{SC} (mA cm^{-2})	FF (%)	PCE (%)	E_{DA} (eV)	E_{CT}[a] (eV)	E_b (eV)	E_a[b] (meV)
PCBM//P3DDFT/P3HT	0.62 (0.03)	0.67 (0.05)	0.550 (0.043)	0.227 (0.022)	1.79	1.13 (0.02)	0.66	14.4 (2.1)
PCBM//P3BT-F_{17}/P3HT	0.42 (0.02)	1.03 (0.10)	0.633 (0.009)	0.270 (0.024)	1.29	0.95 (0.01)	0.34	6.9 (0.7)

Values in parentheses are standard deviations. [a]CTS energy extrapolated from the fitting curve of the temperature dependence of V_{OC}. [b]Charge generation activation energy obtained from the temperature dependence of J_{SC}.

absorption spectroscopy in reflectance mode was performed on the films with the device architecture and the results are shown in Figure 5c. Compared with PCBM//P3DDFT/P3HT, PCBM//P3BT-F_{17}/P3HT showed much smaller absorption in the region of the vibronic peaks from the polythiophenes at 550 and 600 nm. This result is consistent with the end-on orientation of the polymer chains, as discussed for the transmission absorption spectra in Figure 2c. Based on the EQE and absorption spectra, internal quantum efficiency (IQE) was calculated (Figure 5d). The PCBM//P3BT-F_{17}/P3HT device had a much higher IQE over the entire spectrum than the PCBM//P3DDFT/P3HT device, indicating superior charge generation at the D/A interface with the end-on oriented polymer chains.

To elucidate the effects of the chain orientation on the charge separation process, temperature-dependent J_{SC} measurements were performed on two PHJ devices from −40 to 20 °C. The observed J_{SC} was fitted by the Arrhenius equation[27, 60]

$$J_{SC} = J_0 \exp(-E_a/kT) \quad (3)$$

where J_0 is the preexponential factor, k is the Boltzmann constant, and E_a is the activation energy reflecting the energetic depth of the trapping of the Coulombic interaction at the D/A interface.[27, 60] The measured ln(J_{SC})-1/T relationships were well fit by linear functions (Figure S15) and the E_a values obtained from the slopes are summarized in Table 1. Compared with the PCBM//P3DDFT/P3HT device, the temperature dependence of J_{SC} for the PCBM//P3BT-F_{17}/P3HT device was weaker, indicating lower E_a. The lower E_a of the PCBM//P3BT-F_{17}/P3HT device suggests that the end-on oriented polymer chains at the D/A interface helped to suppress the geminate recombination loss in the device. This suppression could also contribute to the higher fill factor (FF) in the PCBM//P3BT-F_{17}/P3HT device (Figure 5a and Table 1). Although higher hole mobility was expected for the PCBM//P3BT-F_{17}/P3HT device through intrachain charge transport, as previously reported,[40, 61] this factor could not be the main reason for the increased J_{SC} and FF in the PHJ device because the polymer film was thin enough to collect the charges efficiently under short-circuit conditions.[27] To support this result, the dependence of J_{SC} on light intensity was measured at room temperature and low temperatures (Figure S16). J_{SC} increased linearly with light intensity for both devices, indicating that the bimolecular recombination loss was negligible under short-circuit conditions in this temperature range. Therefore, the geminate recombination from the CTS formed by photoirradiation was the dominant loss mechanism in the PHJ devices under short-circuit conditions. We concluded that the improved charge separation from the CTS and the suppressed geminate recombination through CTS of the PCBM//P3BT-F_{17}/P3HT device arose from the end-on oriented polymer chains at D/A interface create a large effective distance and weak Coulombic interaction in the CTS (Figure 5e).

We further attempted to separate the charge separation efficiency quantitatively into the primary processes of exciton diffusion, charge transfer, and charge separation. However, this was a challenging task because the decomposition of IQE spectra to each process produced ambiguous results (Sections S7 and S8, see Supporting Information for discussion).

Conclusions

In conclusion, UPS and LEIPS showed that the end-on orientation of poly(3-alkylthiophene) in films altered the energy structures through the orientation dependence of the polarization energy. The results for OSCs based on the PHJs indicated that the polymer chains with the end-on orientation at the D/A interface produced a lower voltage loss from E_{DA} and better charge generation efficiency. The intrachain delocalization of the holes vertical to the D/A interface weakened the Coulombic interaction in the interfacial CTS and improved the charge separation. Achieving an end-on orientation at the D/A interfaces in BHJ structures is a huge challenge,[62] although it would produce highly efficient charge separation with a much lower energetic driving force.

Experimental

Materials

P3BT-F_{17} and P3DDFT were synthesized following previously reported methods.[44-45] The number average molecular weights of P3BT-F_{17}, P3DDFT, and P3HT were 6000, 8400, and 9200 with polydispersity indices of 1.08, 1.27, and 1.12, respectively, measured by gel permeation chromatography. PCBM (99.5%) was purchased from Solenne.

Device fabrication

For each device, a patterned ITO-coated glass substrate was cleaned by sequential ultrasonication in detergent solution, water, 2-propanol, and acetone, followed by UV-O_3 treatment. Zinc acetate (100 mg) and 2-amine ethanol (28.4 µL) (both from Wako) were dissolved in ethanol (1.6 mL), stirred for 4 h, spin-coated on ITO substrates at 3000 rpm for 30 s, and then dried at 200 °C for 1 h to form the ZnO interfacial layer. After the formation of ZnO, PCBM in chlorobenzene (10 mg mL^{-1}) was spin-coated onto the ZnO layer on the ITO substrates at 600 rpm for 60s. $CHCl_3$ solutions of P3HT (7.6 mg mL^{-1}), P3BT-F_{17} (2.6 mg mL^{-1})/P3HT (5 mg mL^{-1}) and P3DDFT (0.6 mg mL^{-1})/P3HT were spin-coated on glass/poly(*p*-styrenesulfonate sodium salt) (PSS) substrates at 1500 rpm for 60 s. PSS was a sacrificial layer and prepared by spin coating an aqueous solution of PSS (30 mg mL^{-1}) at 3000 rpm for 30 s on glass substrates. Pre-annealing was performed at 60 °C for 12 h, and then at 165 °C for 2 h before transfer. The glass/PSS/polymer substrate was gently placed upside down on the ITO/ZnO/PCBM substrate, and one drop of water was placed on the edge of the two substrates. Water selectively penetrated into and dissolved the PSS layer, allowing the polymer layer to be transferred onto the PCBM layer. A MoO_3 hole-transporting layer (10 nm) and Ag electrodes (80 nm) were deposited by thermal evaporation under high vacuum (~10^{-4} Pa) through a metal mask.

All the samples were encapsulated with a glass cap and UV-curable resin in a dry N_2-filled glovebox.

Measurements

The XPS analysis was performed with a surface analysis instrument (PHI 5000 VersaProbe II, ULVAC-PHI). Monochromatized Al Kα (photon energy 1486.6 eV) radiation was used for all the measurements. The XRD and XRR analyses were performed on an X-ray diffractometer (SmartLab, Rigaku) with monochromatized Cu Kα radiation (λ = 0.154 nm) generated at 45 kV and 200 mA with an incident angle of 0.2°. The reflection patterns were fitted by using GlobalFit software (Rigaku). The 2D GIWAXS analyses were performed at the BL46XU beamline of SPring-8 with an X-ray energy of 12.39 keV. The incident angle of the measurements was fixed at 0.12° using a Huber diffractometer and the 2D GIWAXS pattern was obtained using a 2D image detector (Pilatus 300K, Dectris). Absorption spectra in transmission mode were measured with a UV-Vis spectrophotometer (V-670, JASCO). AFM images were obtained with a scanning probe microscope (5400, Agilent Technologies) in tapping mode. UPS was performed on a surface analysis instrument (PHI5000 VersaProbe II, ULVAC-PHI Inc.) with He(I) excitation (photon energy 21.2 eV). For all UPS measurements, samples were prepared on ITO substrates and a −5 V bias was applied. The UPS analyses were performed at RIKEN, Wako, Japan and the same samples were subsequently sent to Chiba University, Chiba, Japan for the LEIPS measurements. The LEIPS setup has been described elsewhere.[63-64] The low-energy electron beam with kinetic energy in the range of 0–4 eV was incident to the sample surface and the emitted photons were detected by a photon detector equipped with an optical band-pass filter and a photomultiplier tube. The center wavelengths of the band-pass filter were 260, 285, and 335 nm. The overall resolution was approximately 0.3 eV. The *J-V* characteristics of the devices were measured under simulated solar illumination (AM 1.5, 100 mW cm^{-2}). The light intensity was calibrated with a standard silicon solar cell (BS520, Bunkoh-Keiki). The active area of each device was defined by using a 0.12 cm^2 metal photo mask. The EQE of each device was measured with monochromatic light (SM-250F, Bunkoh-Keiki). The transmittance and reflective UV-vis spectra were obtained on a spectrophotometer (V-670, JASCO) equipped with an integrating sphere. The temperature dependences of the *J-V* characteristics of the devices were measured under white LED light at an operation power of 3.4 W (10W LED XM-L, Cree) using a source meter (2400, Keithley).

Conflicts of interest

There are no conflicts to declare.

Acknowledgements

This research was supported in part by Precursory Research for Embryonic Science and Technology (PRESTO), Japan Science and Technology Agency (JST), and the Futaba Electronics Memorial Foundation. GIWAXS experiments were performed at beamline BL46XU of SPring-8 with the approval of the Japan Synchrotron Radiation Research Institute (JASRI; Proposals 2015A1952, 2015A1696, and 2015B1904). F.W. thanks the Junior Research Associate (JRA) program of RIKEN for financial support.

Notes and references

1 Deng, D., et al., Fluorination-Enabled Optimal Morphology Leads to over 11% Efficiency for Inverted Small-Molecule Organic Solar Cells. *Nat. Commun.* **2016**, *7*, 13740.

2 Zhang, G.; Zhang, K.; Yin, Q.; Jiang, X. F.; Wang, Z.; Xin, J.; Ma, W.; Yan, H.; Huang, F.; Cao, Y., High-Performance Ternary Organic Solar Cell Enabled by a Thick Active Layer Containing a Liquid Crystalline Small Molecule Donor. *J. Am. Chem. Soc.* **2017**, *139*, 2387-2395.

3 Zhao, J.; Li, Y.; Yang, G.; Jiang, K.; Lin, H.; Ade, H.; Ma, W.; Yan, H., Efficient Organic Solar Cells Processed from Hydrocarbon Solvents. *Nature Energy* **2016**, *1*, 15027.

4 Zhao, W.; Li, S.; Yao, H.; Zhang, S.; Zhang, Y.; Yang, B.; Hou, J., Molecular Optimization Enables over 13% Efficiency in Organic Solar Cells. *J. Am. Chem. Soc.* **2017**, *139*, 7148-7151.

5 Zhao, W.; Qian, D.; Zhang, S.; Li, S.; Inganas, O.; Gao, F.; Hou, J., Fullerene-Free Polymer Solar Cells with over 11% Efficiency and Excellent Thermal Stability. *Adv. Mater.* **2016**, *28*, 4734-9.

6 Linderl, T.; Zechel, T.; Brendel, M.; Moseguí González, D.; Müller-Buschbaum, P.; Pflaum, J.; Brütting, W., Energy Losses in Small-Molecule Organic Photovoltaics. *Adv. Energy Mater.* **2017**, *7*, 1700237.

7 Lin, Y. L.; Fusella, M. A.; Rand, B. P., The Impact of Local Morphology on Organic Donor/Acceptor Charge Transfer States. *Adv. Energy Mater.* **2018**, 1702816.

8 Clarke, T. M.; Durrant, J. R., Charge Photogeneration in Organic Solar Cells. *Chem. Rev.* **2010**, *110*, 6736-6767.

9 Gregg, B. A., Entropy of Charge Separation in Organic Photovoltaic Cells: The Benefit of Higher Dimensionality. *J. Phys. Chem. Lett.* **2011**, *2*, 3013-3015.

10 Nayak, P. K.; Narasimhan, K. L.; Cahen, D., Separating Charges at Organic Interfaces: Effects of Disorder, Hot States, and Electric Field. *J. Phys. Chem. Lett.* **2013**, *4*, 1707-17.

11 Brédas, J.-L.; Norton, J. E.; Cornil, J.; Coropceanu, V., Molecular Understanding of Organic Solar Cells: The Challenges. *Acc. Chem. Res.* **2009**, *42*, 1691-1699.

12 Chen, K.; Barker, A. J.; Reish, M. E.; Gordon, K. C.; Hodgkiss, J. M., Broadband Ultrafast Photoluminescence Spectroscopy Resolves Charge Photogeneration Via Delocalized Hot Excitons in Polymer:Fullerene Photovoltaic Blends. *J. Am. Chem. Soc.* **2013**, *135*, 18502-12.

13 Dimitrov, S. D.; Durrant, J. R., Materials Design Considerations for Charge Generation in Organic Solar Cells. *Chem. Mater.* **2013**, *26*, 616-630.

14 Shoaee, S.; Clarke, T. M.; Huang, C.; Barlow, S.; Marder, S. R.; Heeney, M.; McCulloch, I.; Durrant, J. R., Acceptor Energy Level Control of Charge Photogeneration in Organic Donor/Acceptor Blends. *J. Am. Chem. Soc.* **2010**, *132*, 12919-12926.

15 Bernardo, B.; Cheyns, D.; Verreet, B.; Schaller, R. D.; Rand, B. P.; Giebink, N. C., Delocalization and Dielectric Screening of Charge

Transfer States in Organic Photovoltaic Cells. *Nat. Commun.* **2014**, *5*, 3245.
16 Gélinas, S.; Rao, A.; Kumar, A.; Smith, S. L.; Chin, A. W.; Clark, J.; van der Poll, T. S.; Bazan, G. C.; Friend, R. H., Ultrafast Long-Range Charge Separation in Organic Semiconductor Photovoltaic Diodes. *Science* **2014**, *343*, 512.
17 Jakowetz, A. C.; Bohm, M. L.; Sadhanala, A.; Huettner, S.; Rao, A.; Friend, R. H., Visualizing Excitations at Buried Heterojunctions in Organic Semiconductor Blends. *Nature Mater.* **2017**, *16*, 551-557.
18 Jakowetz, A. C.; Bohm, M. L.; Zhang, J.; Sadhanala, A.; Huettner, S.; Bakulin, A. A.; Rao, A.; Friend, R. H., What Controls the Rate of Ultrafast Charge Transfer and Charge Separation Efficiency in Organic Photovoltaic Blends. *J. Am. Chem. Soc.* **2016**, *138*, 11672-9.
19 Tamai, Y.; Fan, Y.; Kim, V. O.; Ziabrev, K.; Rao, A.; Barlow, S.; Marder, S. R.; Friend, R. H.; Menke, S. M., Ultrafast Long-Range Charge Separation in Nonfullerene Organic Solar Cells. *ACS Nano* **2017**, *11*, 12473-12481.
20 Deibel, C.; Strobel, T.; Dyakonov, V., Origin of the Efficient Polaron-Pair Dissociation in Polymer-Fullerene Blends. *Phys Rev Lett* **2009**, *103*, 036402.
21 Nenashev, A. V.; Wiemer, M.; Jansson, F.; Baranovskii, S. D., Theory to Exciton Dissociation at the Interface between a Conjugated Polymer and an Electron Acceptor. *J. Non-Cryst. Solids* **2012**, *358*, 2508-2511.
22 Zusan, A.; Vandewal, K.; Allendorf, B.; Hansen, N. H.; Pflaum, J.; Salleo, A.; Dyakonov, V.; Deibel, C., The Crucial Influence of Fullerene Phases on Photogeneration in Organic Bulk Heterojunction Solar Cells. *Adv. Energy Mater.* **2014**, *4*, 1400922.
23 Heidel, T. D.; Hochbaum, D.; Sussman, J. M.; Singh, V.; Bahlke, M. E.; Hiromi, I.; Lee, J.; Baldo, M. A., Reducing Recombination Losses in Planar Organic Photovoltaic Cells Using Multiple Step Charge Separation. *J. Appl. Phys.* **2011**, *109*, 104502.
24 Lyons, B. P.; Clarke, N.; Groves, C., The Relative Importance of Domain Size, Domain Purity and Domain Interfaces to the Performance of Bulk-Heterojunction Organic Photovoltaics. *Energy Environ. Sci.* **2012**, *5*, 7657-7663.
25 Jamieson, F. C.; Domingo, E. B.; McCarthy-Ward, T.; Heeney, M.; Stingelin, N.; Durrant, J. R., Fullerenecrystallisation as a Key Driver of Charge Separation in Polymer/Fullerene Bulk Heterojunction Solar Cells. *Chem. Sci.* **2012**, *3*, 485-492.
26 Burke, T. M.; McGehee, M. D., How High Local Charge Carrier Mobility and an Energy Cascade in a Three-Phase Bulk Heterojunction Enable >90% Quantum Efficiency. *Adv. Mater.* **2014**, *26*, 1923-8.
27 Izawa, S.; Nakano, K.; Suzuki, K.; Hashimoto, K.; Tajima, K., Dominant Effects of First Monolayer Energetics at Donor/Acceptor Interfaces on Organic Photovoltaics. *Adv. Mater.* **2015**, *27*, 3025-31.
28 Nakano, K.; Suzuki, K.; Chen, Y.; Tajima, K., Roles of Energy/Charge Cascades and Intermixed Layers at Donor/Acceptor Interfaces in Organic Solar Cells. *Sci. Rep.* **2016**, *6*, 29529.
29 Nakano, K.; Tajima, K., Organic Planar Heterojunctions: From Models for Interfaces in Bulk Heterojunctions to High-Performance Solar Cells. *Adv. Mater.* **2017**, *29*.
30 Ngongang Ndjawa, G. O., et al., Impact of Molecular Orientation and Spontaneous Interfacial Mixing on the Performance of Organic Solar Cells. *Chem. Mater.* **2015**, *27*, 5597-5604.
31 Rand, B. P., et al., The Impact of Molecular Orientation on the Photovoltaic Properties of a Phthalocyanine/Fullerene Heterojunction. *Adv. Funct. Mater.* **2012**, *22*, 2987-2995.
32 Ojala, A., et al., Merocyanine/C60 Planar Heterojunction Solar Cells: Effect of Dye Orientation on Exciton Dissociation and Solar Cell Performance. *Adv. Funct. Mater.* **2012**, *22*, 86-96.
33 Jo, S. B.; Kim, H. H.; Lee, H.; Kang, B.; Lee, S.; Sim, M.; Kim, M.; Lee, W. H.; Cho, K., Boosting Photon Harvesting in Organic Solar Cells with Highly Oriented Molecular Crystals Via Graphene–Organic Heterointerface. *ACS Nano* **2015**, *9*, 8206-8219.
34 Ran, N. A.; Roland, S.; Love, J. A.; Savikhin, V.; Takacs, C. J.; Fu, Y. T.; Li, H.; Coropceanu, V.; Liu, X.; Bredas, J. L.; Bazan, G. C.; Toney, M. F.; Neher, D.; Nguyen, T. Q., Impact of interfacial molecular orientation on radiative recombination and charge generation efficiency. *Nat. Commun.* **2017,** *8* (1), 79
35 Zhou, K.; Zhang, R.; Liu, J.; Li, M.; Yu, X.; Xing, R.; Han, Y., Donor/Acceptor Molecular Orientation-Dependent Photovoltaic Performance in All-Polymer Solar Cells. *ACS Appl. Mater. Interfaces* **2015**, *7*, 25352-61.
36 Kitchen, B.; Awartani, O.; Kline, R. J.; McAfee, T.; Ade, H.; O'Connor, B. T., Tuning Open-Circuit Voltage in Organic Solar Cells with Molecular Orientation. *ACS Appl. Mater. Interfaces* **2015**, *7*, 13208-16.
37 Lee, H.; Lee, D.; Sin, D. H.; Kim, S. W.; Jeong, M. S.; Cho, K., Effect of Donor–Acceptor Molecular Orientation on Charge Photogeneration in Organic Solar Cells. *NPG Asia Materials* **2018**.
38 Zhang, R.; Yang, H.; Zhou, K.; Zhang, J.; Yu, X.; Liu, J.; Han, Y., Molecular Orientation and Phase Separation by Controlling Chain Segment and Molecule Movement in P3ht/N2200 Blends. *Macromolecules* **2016**, *49*, 6987-6996.
39 Wei, Q.; Miyanishi, S.; Tajima, K.; Hashimoto, K., Enhanced Charge Transport in Polymer Thin-Film Transistors Prepared by Contact Film Transfer Method. *ACS Appl. Mater. Interfaces* **2009**, *1*, 2660-2666.
40 Ma, J.; Hashimoto, K.; Koganezawa, T.; Tajima, K., End-on Orientation of Semiconducting Polymers in Thin Films Induced by Surface Segregation of Fluoroalkyl Chains. *J. Am. Chem. Soc.* **2013**, *135*, 9644-7.
41 Wang, F.; Hashimoto, K.; Tajima, K., Optical Anisotropy and Strong H-Aggregation of Poly(3-Alkylthiophene) in a Surface Monolayer. *Adv. Mater.* **2015**, *27*, 6014-20.
42 Wang, F.; Hashimoto, K.; Segawa, H.; Tajima, K., Effects of Chain Orientation in Self-Organized Buffer Layers Based on Poly(3-Alkylthiophene)S for Organic Photovoltaics. *ACS Appl. Mater. Interfaces* **2018**, *10*, 8901-8908.
43 Geng, Y.; Wei, Q.; Hashimoto, K.; Tajima, K., Dipole Layer Formation by Surface Segregation of Regioregular Poly(3-Alkylthiophene) with Alternating Alkyl/Semifluoroalkyl Side Chains. *Chem. Mater.* **2011**, *23*, 4257-4263.
44 Geng, Y.; Tajima, K.; Hashimoto, K., Synthesis and Characterizations of Regioregular Poly(3-Alkylthiophene) with Alternating Dodecyl/1h,1h,2h,2h-Perfluorooctyl Side Chains. *Macromol. Rapid Commun.* **2011**, *32*, 1478-83.
45 Ma, J.; Geng, Y.; Hashimoto, K.; Tajima, K., Synthesis and Characterization of End-Functionalized Poly(3-Butylthiophene) with Semifluoroalkyl Chains. *Macromol. Chem. Phys.* **2013**, *214*, 1326-1331.
46 Wei, Q.; Tajima, K.; Hashimoto, K., Bilayer Ambipolar Organic Thin-Film Transistors and Inverters Prepared by the Contact-Film-Transfer Method. *ACS Appl. Mater. Interfaces* **2009**, *1*, 1865-1868.

47 Tada, A.; Geng, Y.; Wei, Q.; Hashimoto, K.; Tajima, K., Tailoring Organic Heterojunction Interfaces in Bilayer Polymer Photovoltaic Devices. *Nature Mater.* **2011**, *10*, 450-5.
48 Yoshida, H.; Yamada, K.; Tsutsumi, J. y.; Sato, N., Complete Description of Ionization Energy and Electron Affinity in Organic Solids: Determining Contributions from Electronic Polarization, Energy Band Dispersion, and Molecular Orientation. *Phys. Rev. B* **2015**, *92*.
49 Yoshida, H., Near-Ultraviolet Inverse Photoemission Spectroscopy Using Ultra-Low Energy Electrons. *Chem. Phys. Lett.* **2012**, *539-540*, 180-185.
50 Yoshida, H., Measuring the Electron Affinity of Organic Solids: An Indispensable New Tool for Organic Electronics. *Anal Bioanal Chem* **2014**, *406*, 2231-7.
51 Zhong, Y.; Izawa, S.; Hashimoto, K.; Tajima, K.; Koganezawa, T.; Yoshida, H., Crystallization-Induced Energy Level Change of [6,6]-Phenyl-C61-Butyric Acid Methyl Ester (Pcbm) Film: Impact of Electronic Polarization Energy. *J. Phys. Chem. C* **2014**, *119*, 23-28.
52 Yoshida, H., Principle and Application of Low Energy Inverse Photoemission Spectroscopy: A New Method for Measuring Unoccupied States of Organic Semiconductors. *Journal of Electron Spectroscopy and Related Phenomena* **2015**, *204*, 116-124.
53 Duhm, S.; Heimel, G.; Salzmann, I.; Glowatzki, H.; Johnson, R. L.; Vollmer, A.; Rabe, J. P.; Koch, N., Orientation-Dependent Ionization Energies and Interface Dipoles in Ordered Molecular Assemblies. *Nature Mater.* **2008**, *7*, 326-32.
54 Chen, W.; Huang, H.; Chen, S.; Huang, Y. L.; Gao, X. Y.; Wee, A. T. S., Molecular Orientation-Dependent Ionization Potential of Organic Thin Films. *Chemistry of Materials* **2008**, *20*, 7017-7021.
55 Yamada, K.; Yanagisawa, S.; Koganezawa, T.; Mase, K.; Sato, N.; Yoshida, H., Impact of the Molecular Quadrupole Moment on Ionization Energy and Electron Affinity of Organic Thin Films: Experimental Determination of Electrostatic Potential and Electronic Polarization Energies. *Physical Review B* **2018**, *97*, 245206.
56 Topham, B. J.; Soos, Z. G., Ionization in Organic Thin Films: Electrostatic Potential, Electronic Polarization, and Dopants in Pentacene Films. *Phys. Rev. B* **2011**, *84*.
57 Poelking, C.; Tietze, M.; Elschner, C.; Olthof, S.; Hertel, D.; Baumeier, B.; Wurthner, F.; Meerholz, K.; Leo, K.; Andrienko, D., Impact of Mesoscale Order on Open-Circuit Voltage in Organic Solar Cells. *Nature Mater.* **2015**, *14*, 434-9.
58 Nakano, K.; Shibamori, T.; Tajima, K., Quantitative Evaluation of Molecular Diffusion in Organic Planar Heterojunctions by Time-of-Flight Secondary Ion Mass Spectroscopy. *ACS Omega* **2018**, *3*, 1522-1528.
59 Oehzelt, M.; Koch, N.; Heimel, G., Organic Semiconductor Density of States Controls the Energy Level Alignment at Electrode Interfaces. *Nat. Commun.* **2014**, *5*, 4174.
60 Riedel, I.; Dyakonov, V., Influence of Electronic Transport Properties of Polymer-Fullerene Blends on the Performance of Bulk Heterojunction Photovoltaic Devices. *Phys. Status Solidi A* **2004**, *201*, 1332-1341.
61 Ma, J.; Hashimoto, K.; Koganezawa, T.; Tajima, K., Enhanced Vertical Carrier Mobility in Poly(3-Alkylthiophene) Thin Films Sandwiched between Self-Assembled Monolayers and Surface-Segregated Layers. *Chem. Commun.* **2014**, *50*, 3627-30.
62 Wang, C.; Nakano, K.; Lee, H. F.; Chen, Y.; Hong, Y.-L.; Nishiyama, Y.; Tajima, K., Intermolecular Arrangement of Fullerene Acceptors Proximal to Semiconducting Polymers in Mixed Bulk Heterojunctions. *Angew. Chem. Int. Ed.* **2018**, *57*, 7034-7039.
63 Yoshida, H., Low-Energy Inverse Photoemission Study on the Electron Affinities of Fullerene Derivatives for Organic Photovoltaic Cells. *J. Phys. Chem. C* **2014**, *118*, 24377-24382.
64 Yoshida, H., Note: Low Energy Inverse Photoemission Spectroscopy Apparatus. *Rev. Sci. Instrum.* **2014**, *85*, 016101.